

## Optically Driven Quantum Dots as Source of Coherent Cavity Phonons: A Proposal for a Phonon Laser Scheme

Julia Kabuss,\* Alexander Carmele, Tobias Brandes, and Andreas Knorr

*Institut für Theoretische Physik, Technische Universität Berlin, Hardenbergstrasse 36, 10623 Berlin, Germany*

(Received 9 December 2011; published 31 July 2012)

We present a microscopically based scheme for the generation of coherent cavity phonons (phonon laser) by an optically driven semiconductor quantum dot coupled to a THz acoustic nanocavity. External laser pump light on an anti-Stokes resonance creates an effective Lambda system within a two-level dot that leads to coherent phonon statistics. We use an inductive equation of motion method to estimate a realistic parameter range for an experimental realization of such phonon lasers. This scheme for the creation of nonequilibrium phonons is robust with respect to radiative and phononic damping and only requires optical Rabi frequencies of the order of the electron-phonon coupling strength.

DOI: 10.1103/PhysRevLett.109.054301

PACS numbers: 43.35.Gk, 73.63.Kv, 74.25.N-

Phonon engineering involving acoustic nanocavities has opened the possibility of controlling and studying phonon statistics [1], with applications like phonon lasers [2,3], using ion traps or coupled microcavities, phonon induced electronic transitions [4], or the realization of mechanical motion at the quantum limit in opto- [5] or nanoelectromechanical [6,7] systems.

Phonon cavities are designed to confine single acoustic cavity modes [8,9], and although there are several experimental challenges in their realization (surface imperfections, anharmonic phonon decay, etc.), promising work on high quality cavities with  $Q$  factors of  $Q = 1000$  has already been achieved by design for semiconductors [10,11]. The wide range of novel applications like light modulation in the UV and THz range [12,13], carrier lifetime reduction [14], and phonon laser action [2,3] by controlling the phonon emission behavior of nanostructures has led to various proposals [15] for phononic devices.

In this Letter, we suggest the coherent optical control [16] of a single cavity phonon mode coupled to a two-level quantum dot (QD) to obtain coherent cavity phonon excitations. The key idea is to drive the QD at the anti-Stokes resonance and thus to generate a Raman transition, where a dressed QD level emits phonons into the acoustic cavity. Our scheme has similarities with models for *photonic lasing* of single atoms [17,18] or circuit QED qubits [19], but instead of incoherent pumping we use an effective Lambda system and coherent light to induce *phonon lasing*. Our applied theoretical methods also allow us to scan regimes with arbitrarily strong coupling parameters far beyond the validity of a rotating wave approximation. We mention that transport experiments in suspended QD structures have already demonstrated strong electron-phonon coupling effects recently [20,21].

*Model.*—As a phonon source, we assume a two-level QD coupled to a single nanocavity phonon mode; compare with Fig. 1. The phonon emission (at a typical wavelength of several nanometers) is controlled by an external

optical laser field, which drives the QD transition at the anti-Stokes resonance (stimulated Raman process). The Hamiltonian therefore describes a coherently driven two-level system with two electronic states  $|v\rangle$  and  $|c\rangle$  coupled to a harmonic oscillator mode with coupling strength  $g$ ,

$$\mathcal{H}(t) = \frac{\hbar\omega_{cv}}{2}\sigma_z + \hbar\omega_{ph}b^\dagger b + \Omega(t)\sigma_x + g\sigma^\dagger\sigma(b^\dagger + b), \quad (1)$$

where  $\sigma_z \equiv |v\rangle\langle v| - |c\rangle\langle c|$ ,  $\sigma_x \equiv |v\rangle\langle c| + |c\rangle\langle v|$ ,  $\sigma \equiv |v\rangle\langle c|$ , and  $b^{(\dagger)}$  are the phononic ladder operators [22]. The driving laser with frequency  $\omega_l$  coherently pumps our system via  $\Omega(t) = \Omega \sin\omega_l t$  and is detuned from the QD resonance  $\omega_{cv}$  by the acoustic cavity frequency  $\omega_{ph}$ , so that the QD is driven at the anti-Stokes position  $\omega_l = \omega_{cv} + \omega_{ph}$ . This way, the driven two-level QD is operated as a  $\Lambda$  system with the three dressed states  $|v, n\rangle$ ,  $|c, n\rangle$ , and  $|c, n+1\rangle$ , where  $n$  denotes a phonon Fock state.

*Method.*—The master equation for the reduced system density operator  $\rho$  belonging to Eq. (1) is given by

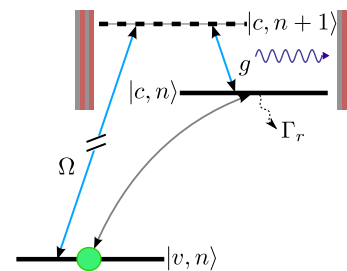


FIG. 1 (color online). Scheme of the QD interacting with an external laser field (Rabi frequency  $\Omega$ ). The QD is assumed as a two-level system with a valence band state  $|v\rangle$  and a conduction band state  $|c\rangle$ . The QD is coupled to a single THz acoustic phonon mode, which is indicated by the multilayered structures.

$$\dot{\rho} = -i[\mathcal{H}(t), \rho] + 2\kappa\mathcal{D}[b]\rho + 2\Gamma_r\mathcal{D}[\sigma]\rho + \frac{\gamma_{pd}}{2}\mathcal{P}[\sigma_z]\rho, \quad (2)$$

where the Lindblad dissipators  $\mathcal{D}[x]\rho \equiv x\rho x^\dagger - \frac{1}{2}\{x^\dagger x, \rho\}$  and  $\mathcal{P}[x]\rho = x\rho x - \rho$  describe intrinsic lifetime effects of the cavity phonon mode  $b$  at the damping rate  $\kappa$ , a radiative damping of the two-level transition at the rate  $\Gamma_r$ , and  $\gamma_{pd}$  as a pure dephasing for a realistic treatment of the semiconductor environment. All corresponding values are chosen from experimental and theoretical data and refer to the low temperature regime ( $T < 100$  K); i.e.,  $\kappa$  and  $\gamma_{pd}$  remain fixed, since the backaction of the electronic and phononic system to a surrounding thermal heat bath can be neglected. Instead of taking matrix elements of Eq. (1) and solving the resulting large system of coupled equations directly, we employ a numerically efficient inductive Heisenberg equation of motion approach for the phonon correlations of necessary order  $\langle b^{\dagger n} b^n \rangle$  ( $n \geq 1$ ), where the brackets denote the trace with the density operator at time  $t$  [23]. This allows us to calculate the time-dependent phonon number probabilities  $P_n(t)$  via a reverse recursion:

$$P_n(t) = \frac{1}{n!} \left( \langle b^{\dagger n} b^n \rangle - \sum_{j=1}^{N_{\text{end}}} \frac{(n+j)!}{j!} P_{n+j}^{\text{ph}} \right), \quad (3)$$

where  $N_{\text{end}}$  is the truncation point of the sum (highest included correlation degree).  $N_{\text{end}}$  has to be chosen according to the initial conditions, parameters, and coupling strengths until convergence is achieved.

Alternatively, it is possible to directly calculate the phonon number probabilities  $P_n = \langle |n\rangle\langle n| \rangle$  via the matrix elements [24] to the phononic density matrix, and then extract the phonon correlations. Here, we choose the equation of motion method for easier access to quantities like the phonon number or phonon-phonon correlation function, and the possibility of a convenient generalization to many-particle systems. Within our equation of motion approach [23,25], which directly gives access to the phonon correlations  $\langle b^{\dagger n} b^n \rangle$ , we derive a set of equations for the phonon-correlated electronic densities  $V^{(n|m)} \equiv |v\rangle \times \langle v| b^{\dagger n} b^m$ ,  $C^{(n|m)} \equiv |c\rangle\langle c| b^{\dagger n} b^m$ , and the polarization  $P^{(n|m)} \equiv |v\rangle\langle c| b^{\dagger n} b^m$ , which for  $n, m \geq 0$  fulfill the following equations of motion:

$$\frac{d}{dt} \langle V^{(n|m)} \rangle = i[(n-m)\omega_{\text{ph}} - i(n+m)\kappa] \langle V^{(n|m)} \rangle + 2\Gamma_r \langle C^{(n|m)} \rangle + i\tilde{\Omega}(t) \langle P^{(n|m)} \rangle - i[\tilde{\Omega}(t) \langle P^{(m|n)} \rangle]^*, \quad (4)$$

$$\begin{aligned} \frac{d}{dt} \langle C^{(n|m)} \rangle &= i[(n-m)\omega_{\text{ph}}] \langle C^{(n|m)} \rangle - [(n+m)\kappa + 2\Gamma_r] \langle C^{(n|m)} \rangle - i\tilde{\Omega}(t) \langle P^{(n|m)} \rangle + i[\tilde{\Omega}(t) \langle P^{(m|n)} \rangle]^* \\ &+ (1 - \delta_{n|0}) n i g \langle C^{(n-1|m)} \rangle - (1 - \delta_{m|0}) m i g \langle C^{(n|m-1)} \rangle, \end{aligned} \quad (5)$$

$$\begin{aligned} \frac{d}{dt} \langle P^{(n|m)} \rangle &= -i[\omega_{\text{cv}} - (n-m)\omega_{\text{ph}}] \langle P^{(n|m)} \rangle - [(n+m)\kappa + \gamma_p + \Gamma_r] \langle P^{(n|m)} \rangle - i\tilde{\Omega}(t) (\langle C^{(n|m)} \rangle - \langle V^{(n|m)} \rangle) \\ &- i g \langle P^{(n|m+1)} \rangle - i g \langle P^{(n+1|m)} \rangle - (1 - \delta_{m|0}) m i g \langle P^{(n|m-1)} \rangle. \end{aligned} \quad (6)$$

As initial conditions, we assume factorizing thermal phononic and electronic expectation values [26],

$$\langle V^{(n,n)} \rangle(t=0) = \langle V^{(0|0)} \rangle_{\text{th}} \langle b^{\dagger n} b^n \rangle_{\text{th}}, \quad (7)$$

with the phonons in thermal equilibrium and the average phonon number  $n_{\text{ph}} \equiv \langle b^\dagger b \rangle = [\exp(\beta\hbar\omega_{\text{ph}}) - 1]^{-1}$  with  $\beta = (k_B T)^{-1}$ , so that the initial phonon correlation of  $\tilde{n}$ th order  $\langle b^{\dagger \tilde{n}} b^{\tilde{n}} \rangle(0)$  is  $\langle b^{\dagger \tilde{n}} b^{\tilde{n}} \rangle(0) = \tilde{n}!(n_{\text{ph}})^{\tilde{n}}$ . Furthermore,  $\langle V^{(0|0)} \rangle_{\text{th}} = 1$ ; i.e., the electron is initially in the electronic ground state  $|v\rangle$ . All other quantities are zero.

*Results.*—Figure 2(a) shows the temporal evolution of the average phonon number  $\bar{n} \equiv \langle b^\dagger b \rangle$  (solid curve) and the phonon-phonon correlation function  $g_{\text{ph}}^{(2)}(\tau=0) \equiv \langle b^\dagger b^\dagger b b \rangle / \langle b^\dagger b \rangle^2$  (dashed curve). At very short times, i.e., on the scale of the switch-on time of the external pump field (left panel), which is short compared to the time scale given by the electron-phonon coupling and pump field Rabi frequency, the phonons are strongly bunched ( $g_{\text{ph}}^{(2)} \gg 2$ ), starting from a very low phonon number at the initial

temperature ( $T = 4$  K) and the thermal value  $g_{\text{ph}}^{(2)} = 2$ . During the switch-on period, the phonon system is pushed out of the initial thermal equilibrium  $g_{\text{ph}}^{(2)}(0) = 2$ : due to the small initial phonon number, the slightest fluctuation induced by the laser switch-on immediately leads to a large bunching effect. This is followed by a period of time ( $t < 200$  ps) with low  $\bar{n}$  and  $g_{\text{ph}}^{(2)} < 1$  in the *antibunching regime*: due to the continued excitation at the anti-Stokes phonon resonance  $\omega_{\text{cv}} + \omega_{\text{ph}}$ , the electronic population is transferred from the ground to the excited state under phonon emission into the cavity driven by the optically (laser) induced Raman transition. This destroys the thermal equilibrium and results in the generation of Fock state phonon populations. In contrast to this, on a nanosecond time scale [Fig. 2(b)], the phonon number increases and the phonon statistics approach  $g_{\text{ph}}^{(2)} = 1$ , i.e., the coherent limit. This can be explained as follows: for increasing time, in principle, the emitted Fock phonons can be reabsorbed (while the electron is again passing the virtual level

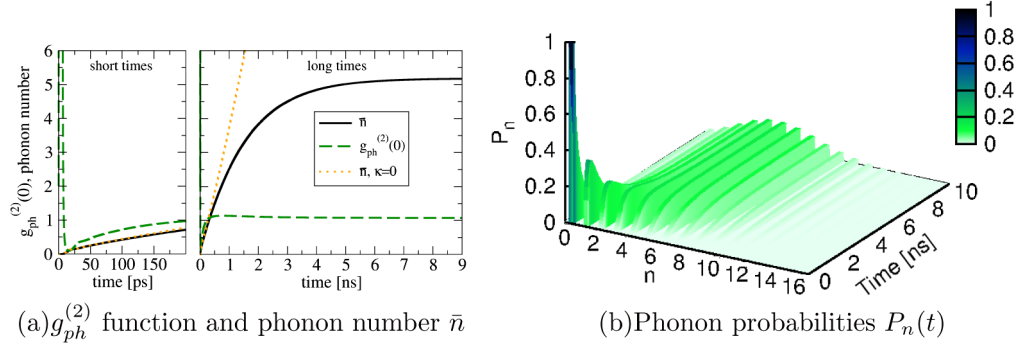


FIG. 2 (color online). (a) Temporal evolution  $\bar{n}$  (solid line) and  $g_{\text{ph}}^{(2)}(0)$  (dashed line). (b) Temporal evolution of  $P_n$  for stationary excitation. Parameters: Rabi frequency  $\Omega = 1.5$  meV, QD-phonon coupling  $|g| = 0.3$  meV [33,34], QD level splitting  $\omega_{\text{cv}} = 1.5$  eV, phonon lifetime  $\kappa^{-1} \equiv 2$  ns [35], QD relaxation rate  $\Gamma_r^{-1} \equiv 200$  ps [36], QD pure dephasing rate  $\Gamma_{\text{pd}}^{-1} \equiv 10$  ps [36], and initial temperature  $T = 4$  K.

$|c, n + 1\rangle$ ). However, eventually the electronic population in the upper level (conduction band density  $C^{(0|0)}$ ) decays by radiative damping  $\Gamma_r$  into the ground state and the previously emitted phonons remain in the cavity; i.e.,  $\bar{n}$  increases. Furthermore, the radiative decay (constant  $\Gamma_r$ ) introduces a random event in the course of time and the repetition of this process leads to randomized phonon statistics, i.e., a transition for a Fock field ( $g^{(2)} < 1$ ) to a more random coherent phonon field with  $g_{\text{ph}}^{(2)}(0)$  values close to 1. The fact that  $g_{\text{ph}}^{(2)}(0)$  converges to the value 1 from above reveals the truly Poissonian character [Fig. 2(b) for long times], representing a coherent phonon state, in contrast to a Fock state with a high phonon number  $g_{\text{ph}}^{(2)}(0) = 1 - 1/\langle b^\dagger b \rangle$ , which is always less than one. We briefly note that the calculated interaction processes are of higher order: from inspection of Eq. (4), the phonon-assisted conduction band density  $C^{(1|0)}$  can be created subsequently, and the (laser) induced Raman process creates higher correlations ( $n, m > 1$ ). Similarly to the coherent phonon population, the phonon-assisted polarizations  $P^{(1|0)}$ ,  $P^{(0|1)}$ , and higher orders in Eq. (6) are crucial for the dynamics.

For comparison, Fig. 2(a) also depicts the evolution of the phonon number without phonon damping  $\kappa = 0$ . In contrast to the case where the phonons are assumed to have a finite lifetime  $\tau = \kappa^{-1}$  and the phonon number  $\bar{n}$  saturates after several nanoseconds (solid line), Fig. 2(a) reveals an exponential rise in slope (dotted line) for  $\bar{n}$ , if an infinite phonon lifetime ( $\kappa \rightarrow 0$ ) is assumed. This kind of increase of  $\bar{n}$  illustrates the characteristic behavior [27] of the intensity caused by stimulated emission, which leads to coherent laser action. To illustrate the temporal evolution of the phonon statistics, the phonon probability distribution  $P_n(t)$  belonging to Fig. 2(a) is shown in Fig. 2(b). At the beginning, the distribution shows thermal Bose-Einstein statistics, with low initial phonon numbers due to the low initial temperature  $T = 4$  K. After switching on the laser, with increasing time the phonon probabilities evolve dynamically into stationary, Poissonian nonequilibrium

statistics. The phonon system then shows the same statistics as photons in a laser. Snapshots of  $P_n$  at  $t = 0$  and  $t = 10$  ns are shown in Fig. 3. The good agreement of the phonon distribution with a real Poissonian distribution is also reflected in the values of the higher order correlation functions  $g^{(n)}(0)$  with  $n > 2$ . Due to the very small fraction of thermal phonons, their deviation from the coherent value 1 is slightly larger than for  $g_{\text{ph}}^{(2)}(0)$ , but less than 5%. This results from a small broadening of the probability distribution in comparison to an exact Poissonian distribution due to a small number of thermal phonons.

*Parameter dependence of coherent phonon regime.*— Clearly, our system allows for phonon laser action characterized by  $g_{\text{ph}}^{(2)} = 1$ , which, however, requires a careful and optimal tuning of parameters. For instance, due to the finite phonon cavity lifetime  $\kappa$ , there is a limit to the phonon number  $\bar{n}$ ; in the present case, the phonon number probabilities with the probability  $P_5$  for finding five phonons have the highest value [see Fig. 2; cf. the snapshot in Fig. 3(b)]. In order to study the dependence of our system on parameters like the excitation strength  $\Omega$ , the phonon lifetime  $\kappa$ , and the radiative loss  $\Gamma_r$  without making any further approximations, the set of Eqs. (4)–(6) is solved numerically in the stationary limit by setting all time derivatives to zero. The results are shown in Fig. 4.

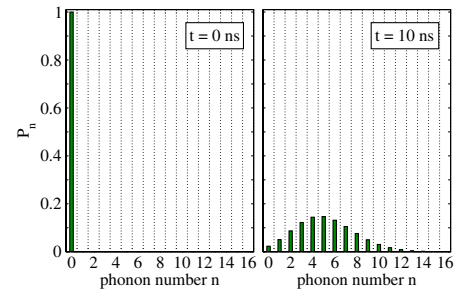


FIG. 3 (color online). Snapshots of the phonon number probabilities  $P_n$  (a) before the optical excitation and (b) in the stationary limit of 1.5 meV.

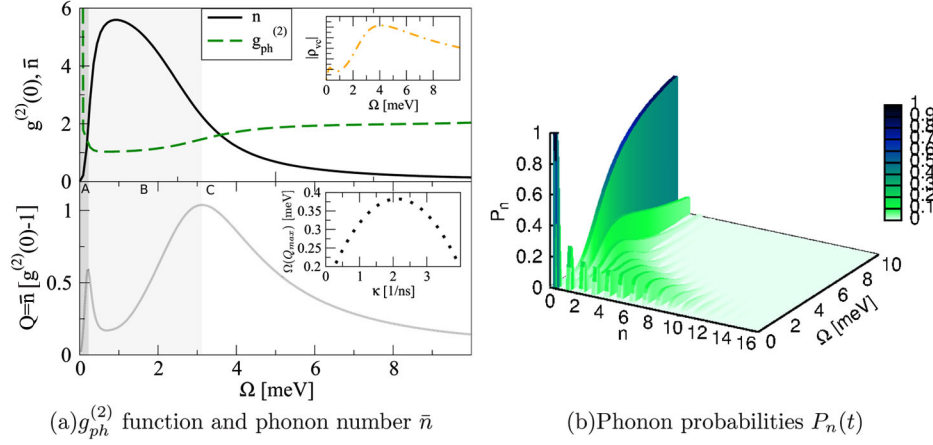


FIG. 4 (color online). (a) Top:  $\bar{n}$  (black solid curve) and  $g_{\text{ph}}^{(2)}(0)$  (dashed curve) over varying laser strength. Excitation dependence of the polarization  $P^{(0|0)}$  (inset: dash-dotted curve). Bottom: evolution of  $Q$  (gray solid curve) and the first *threshold* pump power  $\Omega(Q_{\text{max}})$  (inset: dotted curve) in area A (dark shaded area) over varying phonon damping  $\kappa$ . (b)  $P_n$  over varying laser strength in the stationary regime.

In Fig. 4(a) (top),  $\bar{n}$  and  $g_{\text{ph}}^{(2)}$  are plotted versus rising optical excitation strengths  $\Omega$ , keeping  $\Gamma_r$ , as well as  $\kappa$  fixed at the values used in Fig. 2. Obviously, the system used does not show a clear threshold at lower pump strengths. For the parameter set used, the system stays in the few phonon limit (here,  $n < 6$ ). In this regime, the presence of spontaneous emission leads to a continuous growth of the phonon number and a smooth transition from thermal to coherent phonon emission. The operational *threshold* of the device can be identified by the Mandel- $Q$  parameter  $Q = \bar{n}(g_{\text{ph}}^{(2)} - 1)$  (gray curve), which reflects the deviation from coherent statistics. In Fig. 4(a), three regions (A, B, C), with different emission properties can be identified: in region A, the phonon number and the Mandel- $Q$  parameter are simultaneously increasing. The device is operating in the classical nonlasing regime. At the beginning of region B,  $Q$  has a first maximum (*threshold*), after which the phonon number is increasing, while  $Q$  decreases to a minimum. This simultaneous behavior of  $\bar{n}$  and  $Q$  indicates the coherent laser regime. The dotted curve [inset to Fig. 4(a) (bottom)] shows the first maximum of  $Q$  [threshold:  $\Omega_T := \Omega(Q_{\text{max}})$ ], revealing a nonlinear dependence on  $\kappa$ . Note that there is phonon amplification only during the increase of  $\Omega_T$ . In the regime of  $\kappa$  where  $\Omega_T$  has a negative slope, only low phonon numbers are generated with  $g_{\text{ph}}^{(2)} < 1$  and  $Q < 0$ . Here, the comparably small phonon population, generated via the induced Raman process, is in the Fock state; i.e., the phonon statistics are antibunched. Further, Fig. 4(a) reveals in region C that there is only a limited  $\Omega$  interval (self-quenching), similar to single atom lasers [17,28–31], where coherent phonon populations ( $g_{\text{ph}}^{(2)} = 1$ ) can be established. This can be explained as follows: for pumping strengths  $\Omega < 0.01$  meV, the initial thermal phononic distribution is barely changed. Only very small phonon numbers are achieved, with  $g_{\text{ph}}^{(2)}$  values well in the bunching regime.

However, if the Rabi energy  $\Omega$  reaches values of the order of the electron-phonon coupling strength  $g$ , much higher phonon populations  $\bar{n}$  are generated. In this regime, the external laser pump induced Raman emission process, with the electron passing the virtual intermediate phonon-assisted energy state  $|c, n+1\rangle$ , is dominant, and  $g_{\text{ph}}^{(2)}$  remains close to its coherent value of 1. On the other hand, for Rabi energies  $\Omega \approx \hbar\omega_{\text{ph}}$ , the induced phonon emission process is disabled by the high external laser strength, making coherent phonon emission ineffective, and the phonon system undergoes a strong heating. The  $g_{\text{ph}}^{(2)}$  function then saturates at the value for pure thermal statistics of 2. In this case, the external pump laser is then so strong that the electronic densities are driven by the laser field also resonantly, although the frequency is detuned with respect to the electronic transition  $|v\rangle \rightarrow |c\rangle$ . This is also reflected in the behavior of the microscopic polarization  $|P^{(0|0)}|$  [dash-dotted curve, inset to Fig. 4(a) (top)], which, similar to the Mandel- $Q$  parameter, shows a minimum during the coherent phonon emission. Phonon-assisted transitions via the virtual intermediate states (Fig. 1) are then of minor importance. Since the generation of a phonon population is then

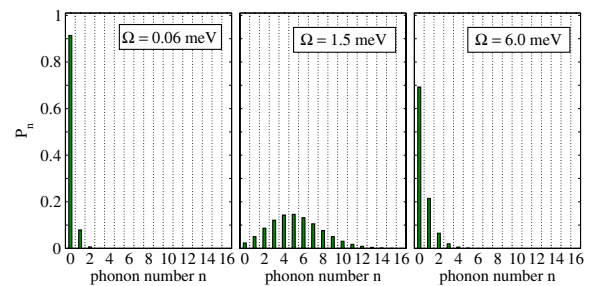


FIG. 5 (color online).  $P_n$  at three different excitation strengths:  $\Omega =$  (a) 0.006 meV, (b) 1.5 meV, and (c) 6 meV.

governed mostly by spontaneous phonon emission, the resulting statistics are thermal.

In order to corroborate this excitation-dependent phonon emission behavior, we plot the phonon probability distributions in Figs. 4(b) and 5. The phonon field is *bunched* for lower excitation strengths  $\Omega = 0.06$  meV and very high excitation strengths  $\Omega = 6.0$  meV. Only in between, when  $\Omega$  is in the range of  $g$ , does the probability distribution  $P_n$  show *Poissonian* phonon statistics [32].

To conclude, we have presented a microscopic equation description of light induced phonon emission from a semiconductor QD coupled to an acoustic THz nanocavity. We found a limited parameter range for the generation of a coherent phonon distribution; in particular, the Rabi frequency  $\Omega$  must be the same order as the electron-phonon coupling strength  $g$ . The presence of a nonphonon related (radiative) decay channel for the electronic densities is crucial for the realization of coherent phonon statistics.

This work is supported by the Deutsche Forschungsgemeinschaft via SFB 910 “Control of self-organizing nonlinear systems: Theoretical methods and concepts of application.”

\*julia@itp.physik.tu-berlin.de

- [1] S. Sauer, J. M. Daniels, D. E. Reiter, T. Kuhn, A. Vagov, and V. M. Axt, *Phys. Rev. Lett.* **105**, 157401 (2010).
- [2] K. Vahala, M. Hermann, S. Knz, V. Batteigner, G. Saathoff, T. W. Hnsch, and T. Udem, *Nature Phys.* **5**, 682 (2009).
- [3] I. S. Grudinin, H. Lee, O. Painter, and K. J. Vahala, *Phys. Rev. Lett.* **104**, 083901 (2010).
- [4] K. J. Ahn, F. Milde, and A. Knorr, *Phys. Rev. Lett.* **98**, 027401 (2007).
- [5] J. Chan, T. P. Mayer Alegre, A. H. Safavi-Naeini, J. T. Hill, A. Krause, S. Grblacher, M. Aspelmeyer, and O. Painter, *Nature (London)* **478**, 89 (2011).
- [6] A. D. O’Connell, M. Hofheinz, M. Ansmann, R. C. Bialczak, M. Lenander, E. Lucero, M. Neeley, D. Sank, H. Wang, M. Weides, J. Wenner, J. M. Martinis, and A. N. Cleland, *Nature (London)* **464**, 697 (2010).
- [7] J. D. Teufel, D. Li, M. S. Allman, K. Cicac, A. J. Sirois, J. D. Whittaker, and R. W. Simmonds, *Nature (London)* **471**, 204 (2011).
- [8] M. Trigo, A. Bruchhausen, A. Fainstein, B. Jusserand, and V. Thierry-Mieg, *Phys. Rev. Lett.* **89**, 227402 (2002).
- [9] Ö. O. Soykal, R. Ruskov, and C. Tahan, *Phys. Rev. Lett.* **107**, 235502 (2011).
- [10] G. Rozas, M. F. Pascual Winter, B. Jusserand, A. Fainstein, B. Perrin, E. Semenova, and A. Lemaître, *Phys. Rev. Lett.* **102**, 015502 (2009).
- [11] N. D. Lanzillotti-Kimura, A. Fainstein, B. Perrin, B. Jusserand, L. Largeau, O. Mauguin, and A. Lemaître, *Phys. Rev. B* **83**, 201103 (2011).
- [12] R. Merlin, *Solid State Commun.* **102**, 207 (1997).
- [13] C. Thomsen, H. T. Grahn, H. J. Maris, and J. Tauc, *Phys. Rev. B* **34**, 4129 (1986).
- [14] J. Chen, J. B. Khurgin, and R. Merlin, *Appl. Phys. Lett.* **80**, 2901 (2002).
- [15] N. D. Lanzillotti-Kimura, A. Fainstein, C. A. Balseiro, and B. Jusserand, *Phys. Rev. B* **75**, 024301 (2007).
- [16] A. Krügel, V. M. Axt, and T. Kuhn, *Phys. Rev. B* **73**, 035302 (2006).
- [17] C. Ginzel, H. J. Briegel, U. Martini, B.-G. Englert, and A. Schenzle, *Phys. Rev. A* **48**, 732 (1993).
- [18] G. M. Meyer, H. J. Briegel, and H. Walther, *Europhys. Lett.* **37**, 317 (1997).
- [19] S. André, P. Q. Jin, V. Brosco, J. H. Cole, A. Romito, A. Shnirman, and G. Schön, *Phys. Rev. A* **82**, 053802 (2010).
- [20] E. M. Weig, R. H. Blick, T. Brandes, J. Kirschbaum, W. Wegscheider, M. Bichler, and J. P. Kotthaus, *Phys. Rev. Lett.* **92**, 046804 (2004).
- [21] R. Leturcq, C. Stampfer, K. Inderbitzin, L. Durrer, C. Hierold, E. Mariani, M. G. Schultz, F. von Oppen, and K. Ensslin, *Nature Phys.* **5**, 327 (2009).
- [22] V. M. Axt, M. Herbst, and T. Kuhn, *Superlattices Microstruct.* **26**, 117 (1999).
- [23] J. Kabuss, A. Carmele, M. Richter, W. W. Chow, and A. Knorr, *Phys. Status Solidi B* **248**, 872 (2011).
- [24] M. Richter, A. Carmele, A. Sitek, and A. Knorr, *Phys. Rev. Lett.* **103**, 087407 (2009).
- [25] A. Carmele, M. Richter, W. W. Chow, and A. Knorr, *Phys. Rev. Lett.* **104**, 156801 (2010).
- [26] H.-P. Breuer and F. Petruccione, *The Theory of Open Quantum Systems* (Oxford University, Oxford, 2002).
- [27] W. H. Louisell, *Quantum Statistical Properties of Radiation* (Wiley, New York, 1973).
- [28] Y. Mu and C. M. Savage, *Phys. Rev. A* **46**, 5944 (1992).
- [29] J. McKeever, A. Boca, A. D. Boozer, J. R. Buck, and H. J. Kimble, *Nature (London)* **425**, 268 (2003).
- [30] F. Dubin, C. Russo, H. G. Barros, A. Stute, C. Becher, P. O. Schmidt, and R. Blatt, *Nature Phys.* **6**, 350 (2010).
- [31] P. Gartner, *Phys. Rev. A* **84**, 053804 (2011).
- [32] As a technical remark, a comparison of Figs. 3(b) and 5(b) also proves that the longtime solution of the dynamically solved equations (computing the full temporal evolution, including initial values for the temperature and the electronic populations) coincides with the stationary limit right away, the latter requiring only electronic population probability conservation.
- [33] E. Stock, M.-R. Dachner, T. Warming, A. Schliwa, A. Lochmann, A. Hoffmann, A. I. Toropov, A. K. Bakarov, I. A. Derebezov, M. Richter, V. A. Haisler, A. Knorr, and D. Bimberg, *Phys. Rev. B* **83**, 041304 (2011).
- [34] The electron-phonon coupling strength is chosen in comparison to Ref. [33]. It can be expected that the coupling strength  $g$  is enhanced for a QD coupled to a phonon cavity.
- [35] P. Lacharmoise, A. Fainstein, B. Jusserand, and V. Thierry-Mieg, *Appl. Phys. Lett.* **84**, 3274 (2004).
- [36] P. Borri, W. Langbein, S. Schneider, U. Woggon, R. L. Sellin, D. Ouyang, and D. Bimberg, *Phys. Rev. Lett.* **87**, 157401 (2001).